Inorg. Chem. **2009**, *48*, 1678−1688

Fe L- and K-edge XAS of Low-Spin Ferric Corrole: Bonding and Reactivity Relative to Low-Spin Ferric Porphyrin

Rosalie K. Hocking,[†,‡] Serena DeBeer George,[*,§] Zeev Gross,[||] F. Ann Walker,[⊥] Keith O. Hodgson,[*,§] Britt Hedman,[*,§] and Edward I. Solomon[*,†]

Department of Chemistry, Stanford University, Stanford, California 94305, Monash Centre for Synchrotron Science and School of Chemistry, Monash University, Australia, 3800, Stanford Synchrotron Radiation Laboratory, SLAC, Stanford University, Stanford, California 94309, Schulich Faculty of Chemistry, Technion - Israel Institute of Technology, Haifa 32000, Israel, and Department of Chemistry, The University of Arizona, Tucson, Arizona 85721

Received November 22, 2008

Corrole is a tetrapyrrolic macrocycle that has one carbon atom less than a porphyrin. The ring contraction reduces the symmetry from D_{4h} to C_{2v}, changes the electronic structure of the heterocycle, and leads to a smaller central cavity with three protons rather than the two of a porphyrin. The differences between ferric corroles and porphyrins lead to a number of differences in reactivity including increased axial ligand lability and a tendency to form 5-coordinate complexes. The electronic structure origin of these differences has been difficult to study experimentally as the dominant porphyrin/corrole $\pi \rightarrow \pi^*$ transitions obscure the electronic transitions of the metal. Recently, we have developed a methodology that allows for the interpretation of the multiplet structure of Fe L-edges in terms of differential orbital covalency (i.e., the differences in mixing of the metal d orbitals with the ligand valence orbitals) using a valence bond configuration interaction model. Herein, we apply this methodology, combined with a ligand field analysis of the Fe K pre-edge to a low-spin ferric corrole, and compare it to a low-spin ferric porphyrin. The experimental results combined with DFT calculations show that the contracted corrole is both a stronger σ donor and a very anisotropic π donor. These differences decrease the bonding interactions with axial ligands and contribute to the increased axial ligand lability and reactivity of ferric corroles relative to ferric porphyrins.

1. Introduction

Iron porphyrin chemistry is important in biological systems due to its relevance to the many processes that involve heme proteins and enzymes.[1,2] Iron corroles are analogues of hemes, having one meso carbon atom less than the porphyrins.[3−6] The ring contraction leads to a smaller central cavity and reduces the symmetry from D_{4h} to C_{2v}. The loss of the meso carbon also means the free base corrole is triprotonic and it usually acts as a trianionic ligand toward metal ions. This leads to a number of differences between corrole and porphyrin, both in their free ligand chemistry as well as the chemistry of their metal complexes. Free corrole ligands are much easier to oxidize than porphyrins to readily form corrole cation radicals, and their metal complexes have shorter equatorial bond lengths and more labile axial ligands. Corrole ligands have also been said to stabilize metal complexes in higher oxidation states relative to porphyrins.[7,8] The most stable Fe corrole complexes are in oxidation states (III) and possibly (IV),[9−11] whereas for Fe porphyrin these are (II) and (III).[12−15] Importantly, iron corroles display quite

* Author to whom correspondence should be addressed. E-mail: debeer@stanford.edu (S.D.G.); hodgson@slac.stanford.edu (K.O.H.); hedman@slac.stanford.edu (B.H.); edward.solomon@stanford.edu (E.I.S.). Fax: 650-725-0259.

† Department of Chemistry, Stanford University.

‡ Monash Centre for Synchrotron Science and School of Chemistry, Monash University.

§ Stanford Synchrotron Radiation Laboratory, SLAC, Stanford University.

|| Schulich Faculty of Chemistry, Technion - Israel Institute of Technology.

⊥ Department of Chemistry, The University of Arizona.

(1) Harris, D. L. *Curr. Opinion. Chem. Biol.* **2001**, *5*, 724–735.
(2) Decker, A.; Solomon, E. I. *Curr. Opin. Chem. Biol.* **2005**, *9*, 152–163.
(3) Nardis, S.; Monti, D.; Paolesse, R. *Mini-Rev Org. Chem.* **2004**, *2*, 355–372.
(4) Gross, Z.; Gray, H. B. *Adv. Synth. Catal.* **2004**, *346*, 165–170.
(5) Gryko, D. T.; Fox, J. P.; Goldberg, D. P. *J. Porphyrins Phthalocyanines* **2004**, *8*, 1091–1105.
(6) Goldberg, D. P. *Acc. Chem. Res.* **2007**, *40*, 626–634.
(7) Golubkov, G.; Gross, Z. *J. Am. Chem. Soc.* **2005**, *127*, 3258–3259.
(8) Golubkov, G.; Gross, Z. *Angew. Chem., Int. Ed.* **2003**, *42*, 4507–4510.

10.1021/ic802248t CCC: $40.75
Published on Web 01/16/2009

unique activity as catalysts for various processes,[16] including the decomposition of reactive oxygen and nitrogen species.[17]

The d-manifold of both iron corrole and porphyrin systems have been difficult to study experimentally because the intense $\pi \rightarrow \pi^*$ electronic transitions of the macrocyclic ring obscure the Fe-based electronic transitions, which would allow a probe of the electronic structure of the metal ion. Fe L-edge X-ray absorption spectroscopy (XAS) probes a number of key bonding interactions that are not accessible using other experimental techniques.[18] The $L_{2,3}$-edge involves $2p \rightarrow 3d$ transitions, which are electric dipole allowed, and given that the 2p orbital is localized on the Fe, L-edge intensity is directly proportional to the Fe d-character in the unoccupied and partially occupied valence orbitals of the metal.[18−21] In addition, the energy shift of the L-edge has contributions from the ligand field splitting of the d orbitals. However, although the Fe $L_{2,3}$-edge spectral shape is sensitive to both the ligand field and d-orbital covalency, these are complicated by $2p^53d^{N+1}$ final state multiplet effects (where N is the number of valence electrons in the ground state), similar to the effects described by the Tanabe Sugano[22] matrices and diagrams for d^N ground states.[21,23]

The sum of these contributions to the spectra can be calculated using the ligand field multiplet model implemented by Thole.[24] In early versions of the model, the effect of covalency on the L-edge spectral shape was only accounted for by the reduction of the Slater integrals associated with electron repulsion, (nephelauxetic effect).[25−27] Later versions of the model included the effects of donor covalency through ligand-to-metal charge transfer (LMCT) mixing. This explicitly allows each symmetry set of d^N and $d^{N+1}\underline{L}$ configurations (where $\underline{L}$ = ligand hole) to mix using a valence bond configuration interaction (VBCI) model.

A methodology has been developed,[21] based on simulations of the multiplet spectral shape, that enables the experimental determination of the covalent delocalization of the different symmetry sets of d-orbitals, called differential orbital covalency (DOC). The technique has been successfully applied to systems where both ligand-to-metal donation and metal-to-ligand back-bonding are present.[21,23]

Recently, we have applied the technique to low-spin Fe(II) and Fe(III) porphyrin systems.[28] Our results for Fe(III) porphyrin show it to be a strong σ-donor and strong π-donor (from porphyrin $3e_g$ to Fe d_{xz}/d_{yz}) with negligible π back-bonding from Fe to porphyrin π^*. Calculations further examined the factors that determine the delocalization of the d_{yz} hole (in low spin d^5) and showed that the hole delocalization is a function of axial ligand orientation. The anisotropy of the π-donor interaction of the ImH ligand (perpendicular to the molecular plane) breaks the degeneracy of the Fe d_{xz}/d_{yz}-based orbitals, which determines the relative mixing of the porphyrinate $3e_g$ orbitals and the nature of the d_π hole. This is the redox active molecular orbital (RAMO), which is important to the electron transfer properties of low-spin ferric porphyrins.[28]

Here, we examine the Fe L- and K-edge spectra of a low-spin Fe(III) corrole [Fe(tpcc)(py)$_2$] relative to a low-spin Fe(III) porphyrin [Fe(tpp)(ImH)$_2$]Cl to experimentally determine the valence delocalization of the Fe d-electrons. The results quantify the bonding differences between porphyrin and corrole, and these electronic structure differences are examined in terms of their effects on corrole relative to porphyrin reactivity.

2. Experimental Section

Sample Prepration. [Fe(tpfc)(py)$_2$] and [Fe(tdcc)(py)$_2$] (where tpfc = 5,10,15-tris(pentafluorophenyl)corrole and tdcc = trianion of 5,10,15-tris-(2,6-dichlorophenyl)corrole)) were obtained by the previously published procedure for insertion iron into free base corroles.[29,30] The yields were in the range 90−95% for pure crystalline materials. [Fe(tpfc)(py)$_2$] and [Fe(tdcc)(py)$_2$] were characterized by ^{1}H NMR, ^{19}F-NMR (for Fe(tpfc)(py)$_2$), MS (DCI$^+$, DCI$^-$), and UV−vis spectroscopy.[29,30] [Fe(tpp)(ImH)$_2$]Cl (where tpp = dianion of meso-tetraphenyl porphyrin) was synthesized and characterized according to published methods.[31−34]

XAS Data Collection and Reduction. Fe L-edge X-ray absorption spectra were recorded at the Stanford Synchrotron Radiation

(9) Simkhovich, L.; Zeev, G. *Inorg. Chem.* **2004**, *2004*, 6136–6138.
(10) Zakharieva, O.; Schenemann, V.; Gerdan, M.; Licoccia, S.; Cai, S.; Walker, F. W.; Trautwein, A. X. *J. Am. Chem. Soc.* **2002**, *124*, 6636–6648.
(11) Walker, F. A.; Licoccia, S.; Polesse, R. J. *J. Inorg. Biochem.* **2006**, *100*, 810–837.
(12) Collman, J. P.; Kaplun, M.; Decreau, R. A. *Dalton Trans.* **2006**, *2006*, 554–559.
(13) Ghosh, A.; Steene, E. *J. Inorg. Biochem.* **2002**, *91*, 423–436.
(14) Ghosh, A. *J. Biol Inorg. Chem.* **2006**, *11*, 712–724.
(15) Gross, Z.; Gray, H. B. *Comm. Inorg. Chem.* **2006**, *27*, 61–72.
(16) Aviv, I.; Gross, Z. *Chem. Commun.* **2007**, 1987–1999.
(17) Mahammed, A.; Gross, Z. *Angew Chem., Int. Ed.* **2006**, *2006*, 6544–6547.
(18) George, S. J.; Lowery, M. D.; Solomon, E. I.; Cramer, S. P. *J. Am. Chem. Soc.* **1993**, *115*, 2968–2969.
(19) Kotani, A.; Okada, K. *Tech. Rep. ISSP, Ser. A* **1992**, 2562.
(20) van der Laan, G.; Zaanen, J.; Sawatzky, G. A.; Karnatak, R.; Esteva, J. M. *Phys. Rev. B* **1986**, *33*, 4253–4263.
(21) Wasinger, E. C.; deGroot, F. M. F.; Hedman, B.; Hodgson, K. O.; Solomon, E. I. *J. Am. Chem. Soc.* **2003**, *125*, 12894–12906.
(22) Sugano S.; Tanabe Y. *Multiplets of Transition-Metal Ions in Crystals*; Academic Press: New York, 1970.
(23) Hocking, R. K.; Wasinger, E. C.; deGroot, F. M. F.; Hodgson, K. O.; Hedman, B.; Solomon, E. I. *J. Am. Chem. Soc.* **2006**, *128*, 10442–10451.
(24) Thole, B. T.; van der Laan, G.; Fuggle, J. C.; Sawatzky, G. A.; Karanatak, R. C.; Esteva, J.-M. *Phys. Rev. B* **1985**, *32*, 5107–5118.
(25) Arrio, M.-A.; Sianctavit, Ph.; Cartier dit Moulin, Ch.; Mallah, T.; Verdaguer, M.; Pellegrin, E.; Chen, C. T. *J. Am. Chem. Soc.* **1996**, *118*, 6422–6427.
(26) Arrio, M.-A.; Scuiller, A.; Sainctavit, Ph.; Cartier dit Moulin, Ch.; Mallah, T.; Verdaguer, M. *J. Am. Chem. Soc.* **1999**, *121*, 6414–6420.
(27) Cartier dit Moulin, Ch.; Villain, F.; Bleuzen, A.; Arrio, M. A.; Sianctavit, C.; Lomenech, C.; Escax, V.; Baudelet, F.; Dartyge, E.; Gallet, J. J.; Verdaguer, M. *J. Am. Chem. Soc.* **2000**, *122*, 6653–6658.
(28) Hocking, R. K.; Wasinger, E. C.; Yan, Y.; DeGroot, F. M. F.; Walker, F. A.; Hodgson, K. O.; Hedman, B.; Solomon, E. I. *J. Am. Chem. Soc.* **2007**, *129*, 113–125.
(29) Simkhovich, L.; Goldberg, I.; Gross, Z. *Inorg. Chem.* **2002**, *41*, 5433–5439.
(30) Simkhovich, L.; Mahammed, A.; Goldberg, I.; Gross, Z. *Chem.—Eur. J.* **2001**, *7*, 1041–1047.
(31) Scheidt, W. R.; Osvath, S. R.; Lee, Y. J. *J. Am. Chem. Soc.* **1987**, *109*, 1958–1963.
(32) Landrum, J.; Coppens, P.; Naiyin, N. *Inorg. Chem.* **1988**, *27*, 482–485.
(33) Collman, J. P.; Hoard, J. L.; Kim, N.; Lang, G.; Reed, C. A. *J. Am. Chem. Soc.* **1975**, *97*, 2676–2681.
(34) Walker, F. A.; Huynh, B. H.; Scheidt, W. R.; Osvath, S. R. *J. Am. Chem. Soc.* **1986**, *108*, 5288–5297.

Laboratory (SSRL) on the 31 pole wiggler beam line 10−1 under ring operating conditions of 50−100 mA and 3GeV. The X-ray energy was selected using a 1000 lines/mm spherical grating monochromator. The beam-line entrance and exit slits were set at 20 μm. All measurements were made at room temperature (298 ± 5 K) and at liquid helium temperatures (20 ± 5 K). Low-temperature measurements minimize the possibility of ligand loss (due to ultrahigh vacuum conditions) and also minimize photodamage. As room-temperature and low-temperature data are (within error) identical, only the room-temperature data are presented. All samples were measured as powders on carbon tape. The energy was calibrated from the Fe L-edge spectrum of Fe_2O_3, run at intervals between scans. The second feature in the L_3 and the first feature in the L_2 edges were calibrated to 708.5 and 720.1 eV, respectively. Data were measured over the range 670−830 eV to permit normalization as described previously.[21] A step size of 0.1 eV was used over the edge region (700−730 eV) and 0.5 eV steps over the remaining regions. A function of the form absorption = $[\tan^{-1}(k(\text{energy} - E_1) + \pi/2)(2/3)(1/\pi)] + [\tan^{-1}(k(\text{energy} - E_2) + \pi/2)(1/3(1/\pi)]$, where $k = 0.295$ as obtained by experimental fit,[21,35] E_1 is the energy of the center of the L_3 edge, and $E_2 = E_1 + 12.3$ eV (the energy split by spin orbit coupling), was used to model the L_3- and L_2-edge jumps, as described previously.[21] The absolute energy of the arctangent was estimated based on a combination of experimental fit and other Fe(III) data.[21,36,37] The L_3 intensity reported here is determined after normalization between 701 and 716 eV and the L_2 intensity after normalization between 716 and 731 eV. The error reported represents an estimate of the error in normalizing spectra obtained during different experimental runs.

Fe K-edges. Fe K-edge data were measured on SSRL beam line 2−3, under the same ring conditions described above. The radiation was monochromatized using a Si(220) double-crystal monochromator. Data were measured in transition mode with N_2-filled ionization chamber to $k = 9.5$. Samples were measured as solids in a boron nitride matrix and maintained at a temperature of 10 K in a helium atmosphere using an Oxford Instruments CF1208 cryostat. Two to three scans were recorded per sample to ensure reproducibility. A two-segment spline of order two was fit to the postedge region, and all data were normalized at 7130 eV.[38] Energies were calibrated using an internal foil standard against the first inflection point at 7111.2 eV.[39]

Fits to the edges were performed using the program *EDG_FIT*.[40] Second-derivative spectra were used as guides to determine the number and positions of peaks. Pre-edge and rising-edge features were modeled by pseudo-Voigt line shapes. For the pre-edge feature, a fixed 1:1 ratio of Lorentzian to Gaussian contributions was used.[41,42] Fits were performed over several energy ranges as reported previously.[38] The reported intensity values and standard deviations are based on the average of all good fits. Normalization procedures can introduce ~3% error in pre-edge peak intensities in addition to the error resulting from the fitting procedure.[43]

Computational Details. DFT Calculations. DFT calculations were performed using a combination of the *ADF*,[44−46] *ORCA*,[47] and *Gaussian03* (revision C.01) programs.[48] The starting structures for the compound $[Fe(tpp)(ImH)_2]^+$ (tpp = tetraphenylporphyrin) was taken from the crystal structure of $[Fe(tpp)(ImH)_2](Cl)\cdot(H_2O)\cdot(CHCl_3)$[49,50] and that of $[Fe(tpc)(py)_2]$ (tpc = 5,10,15-tris(phenyl)-corrole) was taken from the crystal structure of $[Fe(tpfc)py_2]$ (tpfc = 5,10,15-tris(pentafluorophenyl)corrole), where the fluorine groups are replaced by hydrogens.[29] Single-point calculations that employed the *ADF* fragment approach were performed using the exchange functional of Becke[51] and the correlation functional of Perdew (BP86).[52] The frozen core approximation[53] was used for the iron 1s-2p orbitals. For valence orbitals, Slater-type orbital (STO) basis sets of triple-ζ quality were employed with polarization functions on the ligand atoms (3d) and additional valence p orbitals on the metal atoms that is *ADF* basis set IV.[45,46,54] Mulliken population analysis was performed as implemented in *ADF*.[44] A single-point calculation was also performed including implicit solvation, using the conductor-like screening model, (COSMO), with $\varepsilon = 78.8$.[55−57] Nonbonded radii used in this calculation (in Å) were: $N = 1.608$, $H = 1.350$, $C = 1.700$, $O = 1.517$, and Fe = 1.800. Orbital splitting patterns and mixing coefficients including solvation were found to be similar to those calculated using a gas-phase model. Orbital plots were generated using *G-OpenMol*

(35) Yeh, J. J.; Lindau, I. *At. Data Nucl. Data Tables* **1985**, *32*, 1–155.
(36) Smith, S.; Taylor, D. A.; Hillier, I. H.; Vincent, M. A.; Guest, M. F.; MacDowell, A. A.; von Niessen, W.; Urch, D. S. *J. Chem. Soc., Faraday Trans.* **1988**, *84*, 209–217.
(37) Bergknut, L.; Andermann, G.; Haycock, D.; Kasrai, M.; Urch, D. S. *J. Chem. Soc., Faraday Trans.* **1981**, *77*, 1879–1889.
(38) Westre, T. E.; Kennepohl, P.; DeWitt, J. G.; Hedman, B.; Hodgson, K. O.; Solomon, E. I. *J. Am. Chem. Soc.* **1997**, *119*, 6297–6314.
(39) Scott, R. A.; Hahn, J. E.; Doniach, S.; Freeman, H. C.; Hodgson, K. O. *J. Am. Chem. Soc.* **1982**, *104*, 5364–5369.
(40) George, G. N. StanfordSynchrotron Radiation Laboratory, Stanford Linear Accelerator Center, Stanford University, Stanford, CA. : 2001.
(41) Agarwal B. K. In *X-ray Spectrscopy*; Springer-Verlag: Berlin, 1979; p 276.
(42) Lytle, F. W.; Greegor, R. B.; Sandstron, D. R.; Marques, E. C.; Wong, J.; Spiro, C. L.; Huffman, G. P.; Huggins, F. E. *Nucl. Intrum. Methods Phys. Rev.* **1984**, *226*, 542.
(43) DeBeer George, S.; Metz, M.; Szilagyi, R. K.; Wang, H.; Cramer, S. P.; Lu, Y.; Tolman, W. B.; Hedman, B.; Hodgson, K. O.; Solomon, E. I. *J. Am. Chem. Soc.* **2001**, *123*, 5757–5767.
(44) Mulliken, R. S. *J. Chem. Phys.* **1955**, *23*, 1833–1840.
(45) Scientific Computing and Modelling NV. *ADF User's Guide*; SCM: Amsterdam, 1999.
(46) Baerends, E. J.; Berces, A.; Bo, C.; Boerrigter, P. M.; Cavallo, L.; Deng, L.; Dickson, R. M.; Ellis, D. E.; Fan, L.; Fischer, T. H.; Fonseca Guerra, C.; van Gisbergen, S. J. A.; Groaeneveld, J. A.; Gritsenko, O. V.; Harris, F. E.; van den Hoek, P.; Jacobsen, H.; van Kessel, G.; Kootstra, F.; van Lengthe, E.; Osinga, V. P.; Philipsen, P. H. T.; Post, D.; Pye, C. C.; Ravenek, W.; Ros, P.; Schipper, R. T.; Schreckenbach, G.; Snijders, J. G.; Sola, M.; Swerhone, D.; teVelde, G.; Vernooijs, P.; Versluis, L.; Visser, O.; van Wezenbeek, E.; Wiesenekker, G.; Wolff, S. K.; Woo, T. K.; Ziegler, T. *ADF Program System 2000.01;* ADF: Amsterdam, 2000.
(47) Neese F. *ORCA—An ab initio, Density Function and Semiempirical Program Package*; University of Bonn: Bonn, Germany, 2007.
(48) Frisch, M. J.; Trucks, G. W.; Schlegel, H. B.; Scuseria, G. E.; Robb, M. A.; Cheeseman, J. R.; Zakrzewski, V. G.; Montgomery, J. A., Jr.; Stratmann, R. E.; Burant, J. C.; Dapprich, S.; Millam, J. M.; Daniels, A. D.; Kudin, K. N.; Strain, M. C.; Farkas, O.; Tomasi, J.; Barone, V.; Cossi, M.; Cammi, R.; Mennucci, B.; Pomelli, C.; Adamo, C.; Clifford, S.; Ochterski, J.; Petersson, G. A.; Ayala, P. Y.; Cui, Q.; Morokuma, K.; Malick, D. K.; Rabuck, A. D.; Raghavachari, K.; Foresman, J. B.; Cioslowski, J.; Ortiz, J. V.; Baboul, A. G.; Stefanov, B. B.; Liu, G.; Liashenko, A.; Piskorz. P.; Komaromi, I.; Gomperts, R.; Martin, R. L.; Fox, D. J.; Keith, T.; Al-Laham, M. A.; Peng, C. Y.; Nanayakkara, A.; Gonzalez, C.; Challacombe, M.; Gill, P. M. W.; Johnson, B.; Chen, W.; Wong, M. W.; Andres, J. L.; Gonzalez, C.; Head-Gordon, M.; Replogle, E. S.; Pople, J. A. *Gaussian 03*, Revision C.01; Gaussian, Inc.: Wallingford, CT, 2004.
(49) *Note that this structure has two molecules in the unit cell, one with parallel ImH lying over the N−Fe−N axis and the other with them bisecting the two N−Fe−N axes. The structure with the parallel ImH was taken for the calculations described herein.*
(50) Scheidt, W. R.; Osvath, S. R.; Lee, Y. J. *J. Am. Chem. Soc.* **1987**, *109*, 1958–1963.
(51) Becke, A. D. *Phys. Rev. A* **1988**, *38*, 3098–3100.
(52) Perdew, J. P. *Phys. Rev. B* **1986**, *33*, 8822–8824.
(53) Baerends, E. J.; Ellis, D. E.; Ros, P. *Theor. Chim. Acta.* **1972**, *27*, 339–354.
(54) Te Velde, G.; Baerends, E. J.; Fonseca, G. C.; Van Gisbergen, S. J. A.; Snijders, J. G.; Ziegler, T. *J. Comput. Chem.* **2001**, *22*, 931–967.
(55) Klamt, A.; Schuurmann, G. *J. Chem. Soc: Perkin Trans 2* **1993**, 799.
(56) Klamt, A.; Jones, V. *J. Chem. Phys.* **1996**, *105*, 9972.
(57) Klamt, A. *J. Chem. Phys.* **1995**, *99*, 2224.

Version 2.2.[58] *Gaussian* and *ORCA* calculations were done to analyze the d_{xz}/d_{yz} splitting. A third set of calculations was performed to examine bond energies. Gaussian calculations employed the B3LYP exchange-correlation functional[59,60] and the PCM solvation model as implemented by Tomasi and co-workers.[61−63] Optimized geometries of $[Fe(tpp)(ImH)_2]^+$ and $[Fe(tpc)(ImH)_2]$ as well as the compounds $[Fe(tpp)(ImH)]^+$, [Fe(tpc)(ImH)], and ImH were calculated using the B3LYP/ 6-311G* functional/ basis set combination. Energies were obtained by single-point calculations on these structures using the same method but with a larger basis set (6-311++G**). This improvement of the basis set did not change the energies by more than 3 kcal mol^{-1}. Frequency calculations were performed on optimized geometries to ensure that optimized structures were true energy minima and to calculate ΔG. *ORCA* calculations employed the BP86[51,52] functional with a polarized triple-ζ (TZVP) basis set.[64]

Ligand Field Multiplet Calculations. Calculations were performed using the multiplet model implemented by Thole,[24] which employs the atomic theory code developed by Cowan,[65] and the crystal field (i.e., symmetry) code developed by Butler.[66] This approach includes both electronic Coulomb interactions and spin−orbit coupling for each subshell.[12,53] To simulate the spectra, the Slater−Condon−Shortley parameters (F_i and G_i) were first reduced to 80% of their Hartree−Fock calculated values to account for the overestimation of electron−electron repulsion found in ab initio Hartree−Fock calculations of the free ion. The spectrum is calculated from the sum of all possible transitions for an electron excited from the occupied 2p level into an unoccupied 3d level.[54] In the crystal field limit the ground-state is approximated by a single electronic configuration d^N (where, N = the number of valence d electrons) split in energy by electron repulsion and a crystal field potential in D_{4h} symmetry defined by the parameters Dq, Ds, and Dt where the relationships between the orbital energies and the crystal field parameters are: $b_{1g}(d_{x^2-y^2}) = 6Dq + 2Ds - 1Dt$, $a_{1g}(d_{z^2}) = 6Dq - 2Ds - 6Dt$, $b_{2g}(d_{xy}) = -4Dq + 2Ds - 1Dt$, $e_g(d_{xz}/d_{yz}) = -4Dq - 1Ds + 4Dt$.[26,67] For both corrole and porphyrin, the energies of these orbitals were estimated based on DFT calculations. Ground-state energies and eigenfunctions (Kohn−Sham orbitals) were used to correlate to data. Previous studies on molecular systems have shown reasonable empirical correlations between d−d transitions and ground-state d-orbital energy differences,[68−70] which also correlate to TD-DFT calculation results.[71]

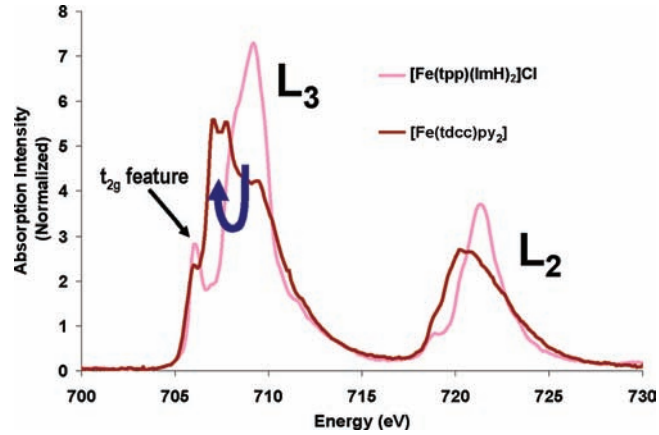

Figure 1. Normalized Fe L-edge absorption for the compounds: $[Fe(tpp)(ImH)_2]Cl$ (porphyrin) and $[Fe(tdcc)py_2]$ (corrole).

Covalent mixing of the metal valence d orbitals with the ligand valence p orbitals was included using a charge transfer model, which in the case of ligand-to-metal charge transfer (LMCT) adds a $d^{N+1}\underline{L}$ configuration energetically above the d^N ground state (by an energy separation Δ). The two states are coupled by configuration interaction (CI), represented by the mixing term $T_i = \langle 3d^N|h|d^{N+1}\underline{L}\rangle$, where h is the molecular Hamiltonian and T_i is proportional to metal−ligand overlap for each of the i symmetry blocks. For a donor ligand system, the ground and LMCT states are $\Psi_{GS,B} = \alpha_1|3d^N\rangle + \beta_1|3d^{N+1}L\rangle$ and $\Psi_{GS,AB} = \beta_1|3d^N\rangle - \alpha_1|3d^{N+1}L\rangle$ and the L-edge excited states are $\Psi_{ES,B} = \alpha_2|2p^53d^{N+1}\rangle + \beta_2|2p^53d^{N+2}L\rangle$ and $\Psi_{ES,AB} = \beta_2|2p^53d^{N+1}\rangle - \alpha_2|2p^53d^{N+2}L\rangle$, where the coefficients α_1, α_2, β_1, and β_2 are a function of T and Δ for the ground-state and T and Δ' for the excited state, where $\Delta' = \Delta_{GS} + U - Q$, and U is the 3d-3d electron repulsion and Q is the 2p-3d repulsion. To simulate the spectra, first the combination of ligand field and multiplet effects was considered, then σ- and π-donation were explicitly included by LMCT simulations. Because the charge transfer model only allows for D_{4h} symmetry and corrole systems are C_{2v}, the artificial d_{xz}/d_{yz} degeneracy tends to produce an intermediate spin ground state rather than the correct low-spin Fe(III) ground state. To keep the system from adopting an intermediate spin ground state, the electron repulsion in the initial state was lowered to 10%. This does not substantially affect the final state spectral shape, which is the L-edge spectrum (Figure S2 of the Supporting Information).

To determine the DOC, the projection method of ref 21 was applied to the simulated spectrum. This method uses the TT-multiplets program to split the intensity of the spectrum into its different symmetry components via 4s → 4p dummy transitions. These values are then degeneracy weighted to obtain the experimental DOC.

3. Results and Analysis

A. Spectroscopy. The Fe L-edge spectrum of the corrole compound $[Fe(tdcc)py_2]$ (red) is shown in Figure 1 with the spectrum of the porphyrin compound $[Fe(tpp)(ImH)_2]Cl$

(58) http://www.csc.fi/gopenmol/distribute/index.phtml.
(59) Lee, C.; Yang, W.; Parr, R. G. *Phys. Rev. B* **1988**, *37*, 785–789.
(60) Becke, A. D. *J. Chem. Phys.* **1993**, *98*, 5648.
(61) Mennucci, B.; Cances, E.; Tomasi, J. *J. Phys. Chem.* **1997**, *B101*, 10506–10507.
(62) Cammi, R.; Mennucci, B.; Tomasi, J. *J. Phys. Chem.* **1999**, *A103*, 9100–9102.
(63) Cammi, R.; Mennucci, B.; Tomasi, J. *J. Phys. Chem. A* **2000**, *104*, 5631–5632.
(64) Schafer, A.; Huber, C.; Ahlrichs, R. *J. Chem. Phys.* **1994**, 100–105.
(65) Cowan R. D. *The Theory of Atomic Structure and Spectra*; University of California Press: Berkeley, 1981.
(66) Butler P. H. *Point Group Symmetry, Applications, Methods and Tables*; New York, 1991.
(67) van der Laan, G.; Kirkman, I. W. *J. Phys.: Condens. Matter* **1992**, *4*, 4189–4204.
(68) Gorelsky, S. I.; Basumallick, L.; Vura-Weis, J.; Sarangi, R.; Hodgson, K. O.; Hedman, B.; Fujisawa, K.; Solomon, E. I. *Inorg. Chem.* **2005**, *44*, 4947–4960.
(69) Basumallick, L.; Sarangi, R.; Debeer George, S.; Elmore, B.; Hooper, A. B.; Hedman, B.; Hodgson, K. O.; Solomon, E. I. *J. Am. Chem. Soc.* **2005**, 3531–3544.
(70) Solomon, E. I.; Szilagyi, R. K.; Debeer George, S.; Basumallick, L. *Chem. Rev.* **2004**, *2004*, 419–458.
(71) Bianconi, A.; Della Longa, S.; Li, C.; Pompa, M.; Congui-Castelllano, A.; Udron, D.; Flank, A.-M.; Lagarde, P. *Phys. Rev. B* **1991**, *44*, 10126–10138.

Table 1. Summary of Fe L-Edge Experimental Data and Results for [Fe(tpp)(ImH)$_2$]Cl (Ferric porphyrin) and [Fe(tpc)(ImH)$_2$] (Ferric Corrole)

	Fe−X distance (Å)	total intensity	% metal character summed over unoccupied orbitals[a]	% average metal character in unoccupied orbitals[a]	L_3 area	L_2 area	branching ratio $L_3/(L_2 + L_3)$
[Fe(tpp)(ImH)$_2$]Cl	Fe−N = 1.992	38.3	303(27)	61(6)	26.3	12.0	0.69
Fe^{III} porphyrin	Fe−N(ImH) = 1.964[50]	(2.5)		As Fe(III)			
[Fe(tpc)(py)$_2$]	Fe−N = 1.886	37.4	295(20)	57(4)	25.1	12.3	0.67
Fe^{III}corrole	Fe−N(py) = 2.031[29]	(2.5)		As Fe(III)			

[a] The percent metal character summed over unoccupied orbitals reflects the combined effects of covalency and back-bonding. In a system with no back-bonding, this number divided by the number of holes gives the percent metal character in each orbital. For [Fe(tpp)(ImH)$_2$]Cl, 303/5 = 61 as given in column 4, line 1.

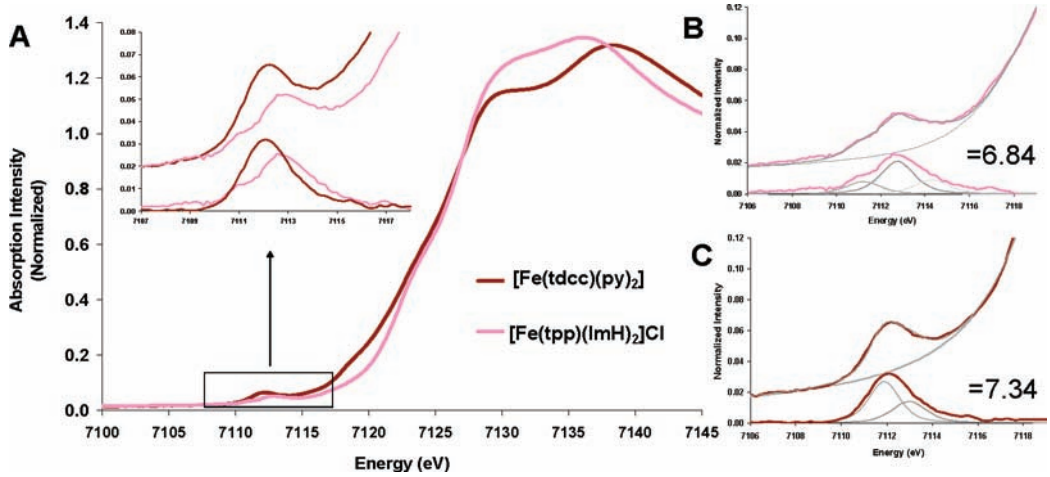

Figure 2. A. Normalized Fe K-edge absorption spectra for [Fe(tpp)(ImH)$_2$]Cl (porphyrin) and [Fe(tdcc)py$_2$] (corrole). The inset shows an expansion of the Fe K pre-edges and the background subtracted Fe K pre-edge. B. Fe(III) porphyrin pre-edge showing a fit to the data (gray) and background subtracted pre-edge. C. Fe(III) corrole pre-edge showing a fit to the data (gray) and background subtracted data.

(pink) from ref 28 included for comparison.[72] Spectral intensities can be integrated to obtain the total covalency using the method described in ref 21. This gives the covalency averaged over the unoccupied Fe_{3d} orbitals for ferric porphyrin to be 61(6)% and for ferric corrole to be 57(4)%, within the same error (Table 1). The main peak of the corrole L_3 spectrum at ~709 eV is significantly broader than the ferric porphyrin spectrum, and the intensity in the corrole spectrum redistributes to the lower energy part of the main peak, indicated by the curved blue arrow. The t_{2g} feature (the feature to lowest energy arising from the $2p^6t_{2g}{}^5 \rightarrow 2p^5t_{2g}{}^6$ transition), (indicated by the black arrow in Figure 1) decreases in intensity relative to the main feature (mostly $2p^6t_{2g}{}^5 \rightarrow 2p^5t_{2g}{}^5e_g{}^1$ (labeled e_g multiplet)) and is no longer separated from the main transition envelope.

Fe K-edge spectra are included for comparison with the Fe L-edge data. Part A of Figure 2 shows the normalized Fe K-edge spectrum of Fe(III) corrole, [Fe(tdcc)py$_2$] (red) compared to that of Fe(III) porphyrin, [Fe(tpp)(ImH)$_2$]Cl (pink), including an inset that magnifies the pre-edge region. Parts B and C of Figure 2 show representative fits to the pre-edges of [Fe(tdcc)(py)$_2$] and [Fe(tpp)(ImH)$_2$]Cl, respectively. The Fe K pre-edge spectrum has similar information to that of the L-edge in that both involve transitions to the Fe d-orbitals so that the shapes and energies of both exhibit effects of the ligand field. However, the intensity mechanisms of the two are different. The Fe L-edge $Fe_{2p} \rightarrow Fe_{3d}$ transition is electric dipole allowed, whereas the Fe K pre-edge $Fe_{1s} \rightarrow Fe_{3d}$ transition is electric dipole forbidden. This means that Fe K pre-edge intensity represents the sum of the weaker quadrupole allowed $Fe_{1s} \rightarrow Fe_{3d}$ contributions and stronger electric dipole allowed $Fe_{1s} \rightarrow Fe_{4p}$ contributions, which arise from the low-symmetry mixing of Fe_{4p} character into the Fe_{3d} orbitals. In both $[Fe(tpp)(ImH)_2]^+$ fragments in the crystal structure of $[Fe(tpp)(ImH)_2](Cl)\cdot(H_2O)\cdot(CHCl_3)$,[50] the Fe is close to centrosymmetric; hence, the total intensity part B of Figure 2 (6.8 units) is close to the quadrupole limit.[38,70] There is a small increase in intensity upon going from the porphyrin to the corrole (0.5 units to 7.3, part C of Figure 2). This indicates that the corrole pre-edge intensity is also dominated by a $Fe_{1s} \rightarrow Fe_{3d}$ quadrupole mechanism. The corrole Fe K pre-edge also has a somewhat different shape relative to the porphyrin in that, similar to the L_3-edge, there is more intensity to lower energy (inset in Figure 2). The Fe^{III} L- and K-edges are analyzed in section C.

B. DFT Calculations.

1. Porphyrin vs Corrole Electronic Structure. The porphyrin ligand to a good approximation can be described in D_{4h} symmetry. Upon going to the corrole, the symmetry reduces to C_{2v} due to the contracted ring. The two macrocycles and their orientations in their respective symmetries (D_{4h}, porphyrin; and C_{2v}, corrole) relative to an appropriate set of Cartesian coordinates are given at the top of Figure 3. The porphyrin ligand has four sets of valence orbitals capable of interaction with the metal: an occupied b_{2g} orbital ($6b_{2g}$)

(72) A comparison of the Fe L_3 and L_2 multiplet structure of [Fe(tdcc)py$_2$] and [Fe(tpfc)py$_2$] is given in Figure S1 in the Supporting Information. Because of the presence of the fluorine K-edge just below the Fe L-edge, the Fe(tpfc)(py)$_2$] data cannot be properly normalized. However, the overall multiplet structure is essentially identical, and indicates that there is no substantial contribution from the differences in corrole substitution.

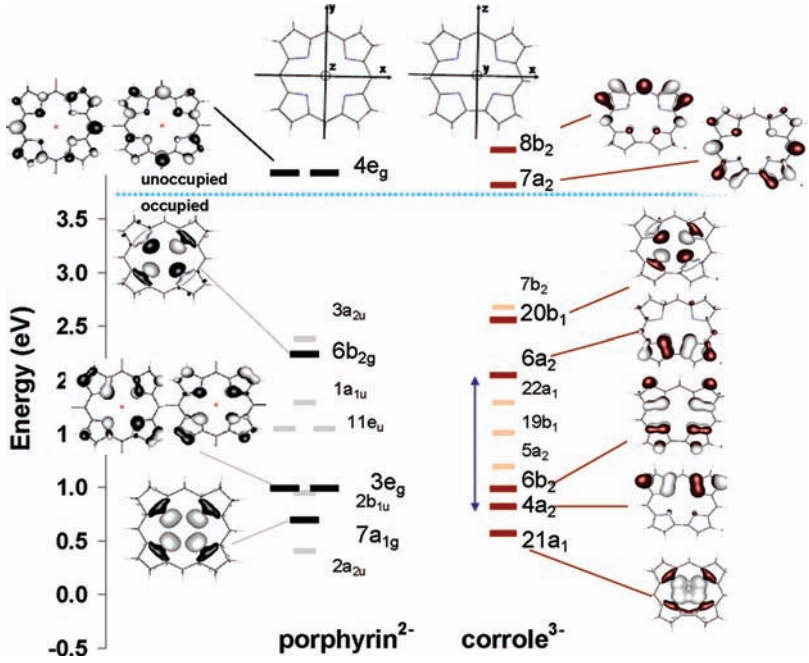

Figure 3. Comparison of the valence orbitals of corrole^{3-} and porphyrin^{2-}. Energy scales are aligned to the C(1s) orbitals. In each case, the molecule is oriented (as shown above) so that the primary rotation axis is *z*. Dark-colored orbitals (black, porphyrin; brown, corrole) are those that interact with the metal, and light-colored orbitals (gray, porphyrin; tan, corrole) are those that cannot. See Figure S6 of the Supporting Information for contours of all of the molecular orbitals; 3.75 eV was subtracted from the corrole scale so as to align the C(1s) orbitals.

capable of σ-donation into the (metal) $d_{x^2-y^2}$, an occupied a_{1g} orbital ($7a_{1g}$) capable of σ-donating to d_{z^2}, an occupied doubly degenerate $3e_g$ orbital set capable of π-donation into unoccupied d_{xz}/d_{yz}, and an unoccupied doubly degenerate $4e_g$ orbital set suitable for π-accepting electrons from occupied Fe d_{xz}/d_{yz} orbitals. The energy levels associated with these orbitals are given in black to the left in Figure 3 (lines in gray indicate u symmetry orbitals which do not interact with the metal unless the D_{4h} symmetry is lowered).[23,73] By correlating the porphyrin D_{4h} orbitals to the C_{2v} symmetry of the corrole, the degeneracy of the $3e_g$ set splits into two levels: one of a_2 and the other of b_2 symmetry. The b_2 orbital is $6b_2$ (Figure 3) and can π-interact with the Fe orbital ($d_{yz} - d_{xz}$). The a_2 orbital from the e_g set mixes with two other a_2 orbitals formed from the b_{1u} and a_{1u} porphyrin orbitals forming three a_2 symmetry orbitals, $4a_2$, $5a_2$ and $6a_2$, of which the $6a_2$ and the $4a_2$ corrole ligand orbitals can interact with the Fe($d_{xz} + d_{yz}$) orbital. These ligand π-donor orbitals are split in energy by ~1.2 eV. The porphyrin $7a_{1g}$ is approximately equivalent to the corrole $21a_1$ and can interact with the Fe d_{z^2} orbital. The corrole- and porphyrin-based orbitals and their nitrogen coefficients are given in Table 2.

Note that in going from the C_{2v} corrole to its Fe complex, we have used a coordinate system that labels the d-orbitals such that the *z* is perpendicular to the corrole plane and the *x* and *y* axes are oriented along the Fe−N bonds but we will continue to use, in the descriptions below, the symmetry labels for the corrole valence orbitals given in Figure 3.

2. ImH and Py Electronic Structures. The compounds considered here have different axial donor ligands; ImH for iron porphyrin and py for iron corrole. ImH has 2p π-donor orbitals (MOs 11 and 13, Figure S7 in the Supporting Information), a σ-donor orbital (MO 12), and a π-acceptor orbital (MO 14). The HOMO/LUMO gap in ImH is 5.7 eV, thus the π^* orbitals are too high in energy to act as π acceptors. Py also has orbitals capable of π-donation (MOs 25A and 26A), σ-donation (MO 29A), and π back-bonding (31A+ 32A). The HOMO−LUMO gap in py is less than in ImH (3.5 eV), making it potentially more effective as a π-acceptor ligand.

Table 2. Percent Nitrogen Contribution to Each Porphyrin (D_{4h}) and Corrole (C_{2v}) Orbitals Capable of Interacting with Fe Obtained from DFT Calculations

$D_{4h} \rightarrow C_{2v}$	porphyrin	corrole
$4e_g \rightarrow 8b_2 + 7a_2$	$4e_g$, 16%	$8b_2$, 9% $7a_2$, 10%
$6b_{2g} \sim 20b_1$	$6b_{2g}$, 79%	$20b_1$, 73%
$3e_g \rightarrow a_2{}^a + 6b_2$	$3e_g$, 38%	$6a_2$, 29%
$1a_{1u} \rightarrow a_2{}^a$	$1a_{1u}$, 0%	$5a_2$, 19%
$1b_{1u} \rightarrow a_2{}^a$	$1b_{1u}$, 15%	$4a_2$, 33% $6b_2$, 35%
$3a_{2u} \rightarrow 7b_2$	$3a_{2u}$, 45%	$7b_2$, 37%
$7a_{1g} \rightarrow 21a_1$	78%	78%

[a] These three a_2 orbitals mix, producing the corrole $4a_2$, $5a_2$, and $6a_2$ orbitals as discussed in the text.

3. Ferric Porphyrin and Corrole Complexes. Figure 4 shows the β-spin molecular orbitals from spin-unrestricted DFT calculations for $[Fe(tpp)(ImH)_2]^+$ (left) and $[Fe(tpc)(py)_2]$ (right). In each case, the five Fe d-orbitals are aligned under one another and the π^* orbitals are offset (to the left for Fe(III) porphyrin, to the right Fe(III) corrole.) The decomposition of the orbitals into their respective fragments using a Mulliken population analysis[44] is given in Table 3. The metal valence orbital at highest energy in both cases is Fe $d_{x^2-y^2}$. In going from Fe porphryin to corrole, the metal character in this orbital decreases from 63(1)% to 59(1) %

(73) Decker, A.; Solomon, E. I. *Angew Chem., Int. Ed.* **2005**, *44*, 2252–2255.

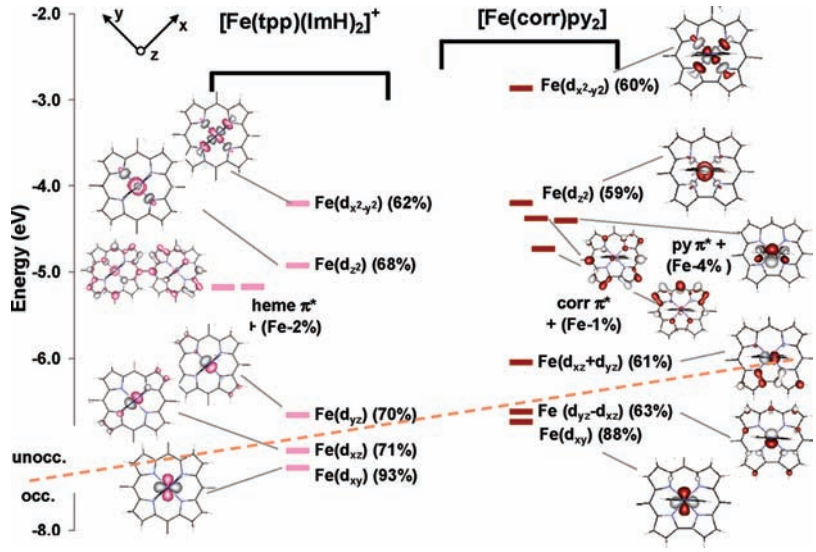

Figure 4. Comparison of the β spin energy levels in $[Fe(tpp)(ImH)_2]^+$ (pink) and $[Fe(tpc)(py)_2]$ (red). In brackets after each orbital is its percent metal character. Note that for the π^* orbitals this number represents only mixing from occupied metal d-orbitals. No occupied metal character was mixed into ImH π^* orbitals for the Fe^{III} porphryin complex, so these orbitals are omitted. Note that 2.75 eV was added to the corrole orbitals to align the C(1s) orbitals. The dotted orange line delineates unoccupied and occupied orbitals.

Table 3. Key Orbital Components from the DFT Calculations for the Fe(III) Complexes $[Fe(tpp)(ImH)_2]Cl$ and $[Fe(tpc)(py)_2]$[a]

main contribution to MO	Fe(III) corrole	Fe(III) porphyrin
Fe ($d_{x^2-y^2}$)	148. 59% (Fe $d_{x^2-y^2}$) + 35% (Corr $-6b_2$) + 1% (py-33A).	77. 62% (Fe $d_{x^2-y^2}$) + 29% (porphyrin $-$ $6b_{2g}$) + 3% (Fe d_{z^2})
Fe (d_z2)	139. 59% Fe(d_{z^2}) + 21% (py-29A σ donor) + 11% (Corr-21a_1) + 5% (py-31A+32A py π acceptor)[b]	76. 68% (Fe d_{z^2}) + 20% (ImH-12) + 7% (porphyrin-7a_{1g})
porphyrin/Corr π-acceptor ($4e_g$)	138/139. 24% 111A + 20% 110A + 15% 108A + 10% 115A + 6%100A)tpc[b] + 3% (Fe d_{xz}/d_{yz})	75. 94% (porphryin $-$ $4e_g$) + 6% (Fe d_{yz}) 74.95%(porphryin $-$ $4e_g$) + 3% (Fe d_{xz})
axial ligand π-acceptor	135. 87% py π acceptor (31A + 32A) + 5% (Fe $d_{yz}-d_{xz}$)	78. 100% ImH π-acceptor (ImH-14)
Fe (d_{xz}/d_{yz})	134. 60% (Fe d_{xz} + d_{yz}) + 25% (Corr-6a_2) + 7% (Corr-4a_2) HOMO/LUMO	73. 70% (Fe d_{yz}) + 20% (porphyrin $-$ $3e_g$) + 2% (porphryin $-$ $4e_g$) 3% (ImH-11) + 2% 4p(x + y)
unoccupied ↑ occupied ↓		
	133. 60% (Fe $d_{yz}-d_{xz}$) + 20% (Corr-6b_2) + 10% (Corr-5a_2)	72. 71% (Fe d_{xz}) + 22% (porphyrin $-$ $3e_g$) + 2% (porphryin $-$ $4e_g$)
Fe(d_{xy})	131. 88% Fe (d_{xy}) + 3% (tpc-77A)	71. 93% Fe(d_{xy})

[a] MO diagrams of the axial Imidazoles (ImH) and pyridines (py) are given in Figures S7 and S8 of the Supporting Information. Bold numbers indicate the orbital number from the ADF calculations. This table is given in the coordinate system of Figure 4. Note that these do not add up to 100% as contributions <1% are not listed. [b] This contribution arises from the fact the py π^* orbitals are close in energy to the d_{z^2} orbital. If $[Fe(tpc)(ImH)_2]$ is used instead (with the axial ligand changed to imidazole), there are no close lying π^* orbital and the Fe character in this orbital is 63%.

and is therefore more covalent. In addition, there is a pronounced increase in the splitting of the Fe d_{z^2} and Fe $d_{x^2-y^2}$ orbitals in going from heme to corrole (0.77 vs 1.35 eV). There are two factors which determine the strength of the bonding interaction: the energy separation of orbitals prior to bonding ΔE, and the matrix element of the molecular Hamiltonian between the metal and ligand orbitals, which is proportional to their overlap integral. In going from heme to corrole, the overlap will increase because the bond lengths are shorter. However, the effect of the energy separation of orbitals prior to bonding must also be considered. To evaluate this contribution, calculations were performed on $[Fe(NH_3)_6]^{3+}$[74] at three different test geometries (six equal $Fe^{III}-N$ distances of 2.00 Å, six equal $Fe^{III}-N$ distances of 1.92 Å and four equatorial bonds at 1.92 Å, and two axial bonds at 2.00 Å (the last are those of the corrole complex)). The ammines model a system where there is little ΔE effect

(74) *Note that in this series of test calculations* $[Fe(NH_3)_6]^{3+}$ *was made low spin.*

Scheme 1

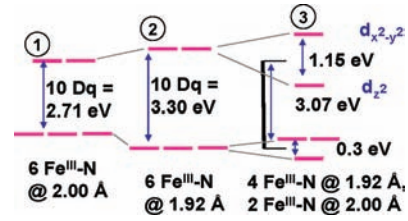

on bonding because the σ donor orbitals of the 6 NH_3 will be close in energy. The results of these calculations are summarized in Scheme 1. The third calculation gives an orbital energy splitting similar to that found for the ferric corrole. Thus, an increase in the overlap at the shorter equatorial distance is sufficient to cause the observed splitting of the Fe $d_{x^2-y^2}$ and d_{z^2} orbitals. Prior to bonding, there is a small offset of the $20b_1$ and $6b_{2g}$ orbitals, of heme and corrole 0.25 eV, in Figure 3 indicating that the ΔE difference between the two prior to bonding are likely to be similar, and their N coefficients are similar (Table 2).[75] After bonding

(Figure S9 of the Supporting Information), the energy separation of the Fe $d_{x^2-y^2}$ to the (corrole) $20b_1$ is ~1.2 eV greater than the separation of Fe $d_{x^2-y^2}$ and $6b_{2g}$ (heme), and the corrole−Fe bond is more covalent (vide infra), reflecting the increased overlap at the shorter equatorial distances due to the ring contraction.

Upon going from iron porphyrin to corrole, the metal based d_{z^2} orbital also decreases in metal character (from 68 to 59%)[61] and is therefore more covalent (Figure 4). There are two sets of ligand-based orbitals that can significantly interact with the Fe d_{z^2} orbital, the porphyrin/corrole based a_{1g} /a_1 orbital and the ImH/py-based σ donor orbital. In the porphyrin system, the a_{1g} orbital has 7% mixing into d_{z^2}. This increases to 11% in the corrole (Table 3). Figure 3 shows that there is no substantial difference in the energy of the porphyrin $7a_{1g}$ and the corrole $21a_1$ orbital, prior to interaction, and Table 2 shows that their *N* coefficients are similar. Thus, the increased d_{z^2} mixing is due to the more efficient overlap with the d_{z^2} lobe in the *xy* plane associated with the shorter Fe−N distances in the iron corrole (1.886 Å[29]) versus porphyrin (1.992 Å[50]).

For a low-spin Fe(III) system, the hole in the t_{2g} (in O_h symmetry) orbital set allows both the porphyrin and the axial ligands to potentially act as π-donors. When both the ImH ligands are aligned along the *x* axis as they are in Figure 4,[76] the out-of-plane ImH π-donor orbitals (MOs 11 and 13, Figure S7 in the Supporting Information) interact with the d_{yz} orbital to destabilize it to become the β-spin LUMO. This orbital (MO 73) contains 20% porphyrin π-donor ($3e_g$) and 3% ImH π-donor character (Table 3). Even though the contribution of the ImH character to the LUMO orbital is relatively small, it is sufficient to significantly split the Fe d_{xz}/d_{yz} (MOs 72 and 73) orbitals in energy by 0.34 eV. This locks in the orientation of the d_π hole so that the axial ImH ligands can π donate (ref 28).

Corrole bonding with Fe differs from porphyrin in that the orbitals capable of π-donation (MOs $4a_2$, $6a_2$, and $6b_2$; Figure 3) are not degenerate before interacting with the Fe. This splitting of the corrole donor orbitals acts to localize the d_π β LUMO of the low-spin Fe(III). The Fe (d_{xz} + d_{yz}) combination mostly interacts with the highest-energy corrole π-donor valence orbital, $6a_2$, localizing the LUMO on the contracted side of the ring. The Fe (d_{yz} − d_{xz}) HOMO is dominated by contributions of the corrole $6b_2$ orbital, (Table 3), distributing it evenly over the ring. On the basis of the orientation of the py rings with respect to the corrole ring (bisecting the *x*,*y* axes parallel to the contracted side of the corrole in Figure 4), they cannot act as π-donors, and, consistent with this, no reciprocal metal character is found in the py π-donor orbitals (MOs 25A and 26A, Figure S8 in the Supporting Information).

For there to be net π back-bonding, occupied metal character must be mixed into unoccupied ligand orbitals and reciprocally ligand π^* mixed into the occupied d_π orbitals. In the Fe(III) corrole, while <2% occupied metal character is mixed into the unoccupied corrole orbitals, about 4% occupied metal character is mixed into py π^* acceptor orbitals. In contrast, for Fe(III) porphyrin there is little occupied metal character (<2%) in either the $4e_g$ π^* or the ImH π^* orbitals.

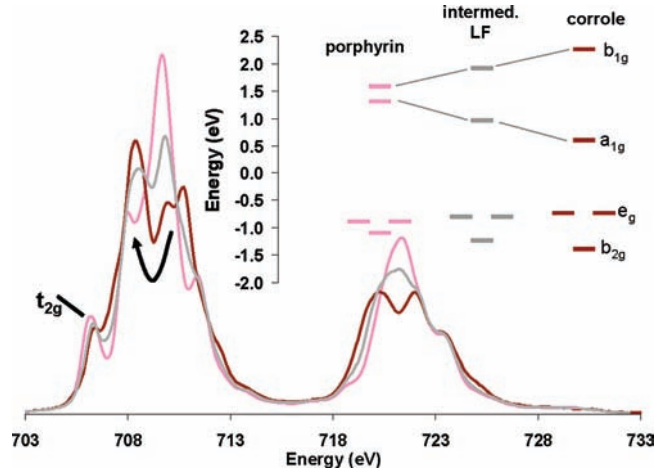

Figure 5. Ionic limit simulations of Fe(III) porphyrin (pink), intermediate ligand field (LF), between porphyrin and corrole) (gray) and Fe(III) corrole (red). Orbital splittings energies (inset) are those calculated based on DFT calculations, with the energy of the e_g orbital set determined by the d_{xz} + d_{yz} hole.

In summary, the DFT calculations show that the large splitting of the d_σ set in corrole relative to porphyrin is due to its very strong tetragonal ligand field due to the short equatorial bond lengths. The d_π LUMO is dominated by the corrole $6a_2$ orbital, which is localized on the contracted side and a sufficiently strong donor to localize the LUMO so as to limit π donation by the axial py.

C. Multiplet and VBCI Analysis of Spectral Shape. Simulations of Fe(III) corrole and porphyrin L-edge spectra performed in D_{4h} symmetry (computational details, multiplets) at the ionic limit using d-orbital energies derived from the DFT calculations are shown in Figure 5. The calculated low-spin Fe(III) porphyrin spectrum is given in pink, the calculated low-spin Fe(III) corrole spectrum is given in red, and the spectrum calculated with an intermediate LF splitting of the d-orbitals is given in gray. The scaled inset shows the relative energies of the three sets of orbitals. From a comparison of the pink and red spectra, the effect of the large splitting of the $d_{x^2-y^2}$ and d_{z^2} orbitals in the Fe(III) corrole is clear. There is a substantial change in the shape of the e_g multiplet consistent with the observed experimental spectral difference in Figure 1. It is also clear that the t_{2g} feature decreases in intensity in going from ferric porphyrin to corrole.

These ionic limit spectra are superposed on the experimental spectra in part A of Figure 6 (Fe(III) corrole) and in Figure S10 of the Supporting Information (for Fe(III) porphyrin and low-spin Fe(III) tacn, included as an innocent ligand analogue). For Fe(III) corrole, the agreement is relatively good. The effects of additional contributions were evaluated: 1) perturbation of the ligand field, 2) differential orbital covalency, and 3) π back-bonding. A slightly

(75) As corrole and porphyrin have different charges, ionic contributions were also considered. The perturbation of the orbital splitting in Scheme 1 by charges equivalent to the NPA population analysis (given in Table S1 in the Supporting Information) was evaluated and the effects were found to be <0.1 eV, an order of magnitude smaller than the effects of ligand−metal d-electron repulsion.

(76) If ImH is the axial ligand, this is 63%.

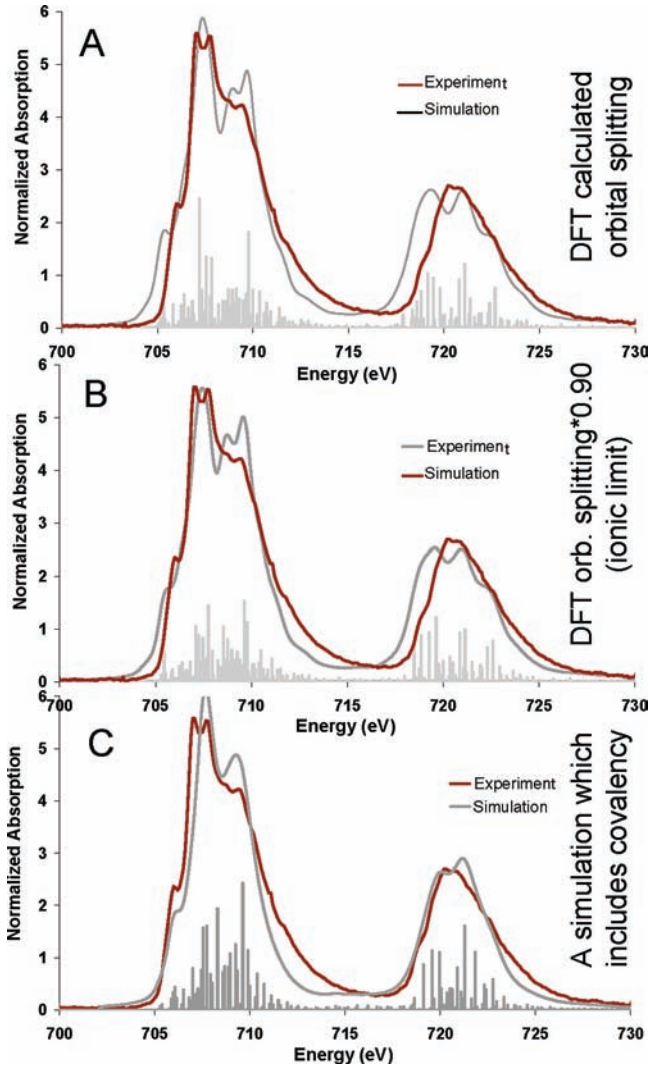

Figure 6. Multiplet and VBCI fits to the Fe(III) corrole L-edge spectrum. A. Fe(III) corrole spectral data superimposed on simulation using the DFT calculated energies. B. Fe(III) corrole spectrum superimposed on simulation with ligand field energies reduced to 90% of the DFT calculated values. C. VBCI fit, which includes covalency. All unoccupied orbitals have equal covalency.

improved fit could be obtained by reducing the ligand field by 10% (part B of Figure 6). The addition of covalency made the spectrum slightly sharper (part C of Figure 6), although no substantial spectral effect reflecting either differential orbital covalency (DOC) or the additional π back-bonding was observed. This is consistent with the DFT calculations in that the $d_{x^2-y^2}$, d_{z^2} and the $d_{xz} + d_{yz}$ orbitals (Figure 4, Table 3) all have about the same covalency, with little π back-bonding. If the covalency of one of the d orbitals were substantially different from the others, a larger difference between the multiplet calculations and those that include

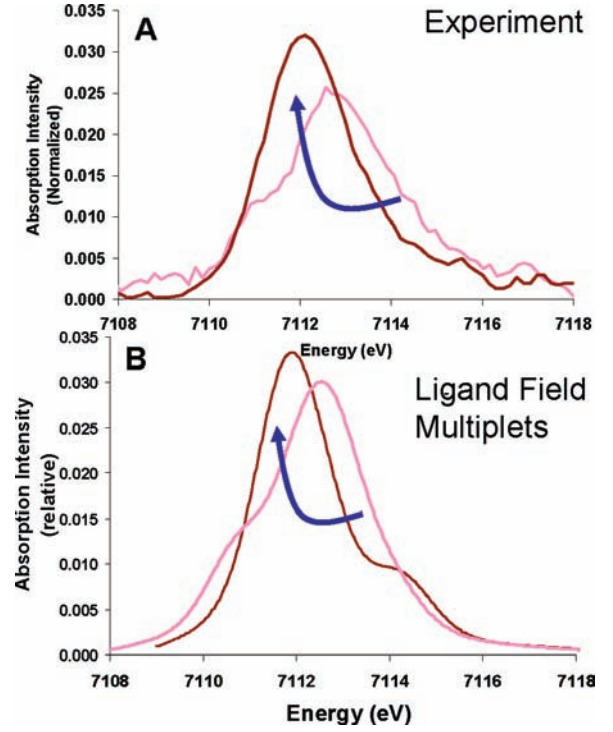

Figure 7. A. Superposition of background subtracted Fe K pre-edges in Fe(III) corrole vs Fe(III) porphyrin. B. Ligand field multiplet simulation of Fe K pre-edges using the parameters in Figure 6. B. (Fe(III) corrole) and in ref 15 (Fe(III) porphyrin).

DOC would be observed, as for $[Fe(tacn)_2]Cl_3$ in Figure S10 of the Supporting Information.

On the basis of the total L-edge intensity, the average metal character in unoccupied orbitals is 57% (Table 1). DFT calculations give 58%, (Table 4) in good agreement with experiment.

In addition to examining L-edge spectral shape, the Fe K pre-edge spectrum can also be simulated with multiplets. The limited intensity observed in the porphyrin and corrole Fe K pre-edge (Figure 2) is characteristic of the dominantly $Fe_{1s} \rightarrow Fe_{3d}$ electric quadrupole character of the transitions (vide supra). Hence, ligand field effects and the splitting of the Fe_{3d} orbitals will dominate the shape of the Fe(III) corrole pre-edge. To evaluate this, the Fe K pre-edges were simulated using the same crystal-field parameters as the Fe L-edges (those in part B of Figure 6, Fe(III) corrole, and ref 15 for Fe(III) porphyrin). These simulations reproduce the redistribution of intensity to lower energy as observed experimentally, (part b of Figure 7) and overall fit the data well, (Figure S11 of the Supporting Information). Also as analyzed for the Fe L-edge (Figure 1), this redistribution in intensity reflects the substantial splitting of the Fe $d_{x^2-y^2}$ and Fe d_{z^2} orbitals.

Table 4. Comparison of the Calculated and Experimental Covalencies for $[Fe(tpp)(ImH)_2]^+$ and $[Fe(tpc)(py)_2]$

				Comparision of VBCI and DFT Values for Differential Orbital Covalency, VBCI(DFT)				
	Total Intensity	% Average Metal Character in Unoccupied Orbitals (Exptl)	% Average Metal Character in Unoccupied Orbitals (Based on DFT)	B1 ($x^2 - y^2$)	A1 (z^2)	B2 (xy)	E1 (xz, yz)	π^* (xz)
A. $[Fe(tpp)(ImH)_2]Cl$ Fe(III)[28]	38.3(2.5)	61(6)	67	54(66)	68(62)	(93)	58(71)	(2)
B. $[Fe(tpc)(py)_2]Fe(III)$	36(2)	57(3)	58	57(58)	57(57)	(82)	57(60)	(<2)

Discussion

The Fe L- and K- pre-edge spectra provide three experimental observables: 1) total intensities, 2) energy shifts, and 3) spectral shapes. The Fe L-edge 2p → 3d transition is electric dipole allowed so the total intensity is directly proportional to the amount of metal character in the unoccupied metal 3d orbitals. The total intensities of the Fe L-edges of Fe(III) corrole and porphyrin are within error the same, indicating that total orbital covalency summed over the unoccupied orbitals of the two complexes are the same. Fe K-edge total intensity can have contributions from strong electric dipole allowed $Fe_{1s} \rightarrow Fe_{4p}$ character, which arises from low-symmetry mixing. However, because the ferric porphyrin compound studied here is close to centrosymmetric, this mixing does not occur, and as the ferric corrole has comparable intensity to the porphyrin, its Fe K pre-edge also has very little 4p character (calculated at 0.3%).[77]

In comparing the Fe L-edge of ferric corrole and ferric porphyrin complexes, the corrole intensity redistributes to lower energy relative to the porphyrin (Figure 1, blue arrow). This same redistribution also occurs in the Fe K pre-edge part a of Figure 7. Ligand field multiplet analyses for both the Fe L-edge and Fe K pre-edge show that this change in spectral shape is caused by a large energy splitting of the Fe $d_{x^2-y^2}$ and d_{z^2} orbitals in ferric corrole relative to ferric porphyrin. Even though these orbitals are substantially split in energy in the Fe(III) corrole, their covalencies are very similar. This is in contrast to Fe(III) porphyrin (ref 15) where the differential orbital covalency analysis showed the Fe $d_{x^2-y^2}$ orbital is more covalent than d_{z^2}. The difference between Fe(III) corrole and porphyrin σ covalency is attributed to the stronger contribution of corrole $21a_1$ (relative to $7a_{1g}$ in the porphyrin, Figure 3) σ donation into the d_{z^2} donut caused by the shorter $Fe^{III}-N$ bond lengths of the Fe(III) corrole.

In the Fe(III) porphyrin, the largest contribution to π donation comes from the $3e_g$ orbitals. As these orbitals are degenerate, they do not split the degeneracy of the Fe d_{xz}/d_{yz} π orbitals. This degeneracy is only split by the orientation of the axial ImH π donor ligands. This can be seen from Figure 8 (first column, pink), which shows that the Fe d_π LUMO is rotated as the ImHs (assumed coplanar) are rotated.

In corrole, the reduction of symmetry from $D_{4h} \rightarrow C_{2v}$ associated with the ring contraction changes the nature of the π donor orbitals from a doubly degenerate set to a set of two nondegenerate a_2 orbitals split by 1.2 eV, $4a_2 + 6a_2$ (Figure 3) (derived from the mixing of one of two porphyrin $3e_g$ orbitals and the a_{1u} and b_{1u} orbitals in C_{2v} symmetry) and the $6b_2$ (derived from the other $3e_g$). This energy splitting is large enough that in a hypothetical [Fe(corrole)$(ImH)_2$] (considered here to eliminate the p back-bonding conritbution of the py studied above), the $d_{xz} + d_{yz}/d_{xz-yz}$ orbitals are split in energy by 0.3−0.5 eV regardless of the orientation of the axial ligands, with the largest splitting occurring when the planar axial ligand bisects the ring-contracted side of the corrole.[78] Hypothetical calculations with an axial NH_3 (σ only donor) show that a 0.3 eV splitting is maintained and thus does not derive from a π-donor interaction with ImH.[78] In all cases, the Fe d_π β LUMO is centered on the ring-contracted side of the corrole. Thus, the corrole ring-contraction locks in the orientation of the Fe d_π β LUMO. This can be seen in Figure 8, right, red, where the d_π β LUMO is antibonding to $6a_2$ and bisects the x and y axes. Thus, in contrast to the Fe(III) porphyrin, in the Fe(III) corrole (red)[79] the Fe d_π β LUMO stays fixed even with changing the orientation of the axial ImH.

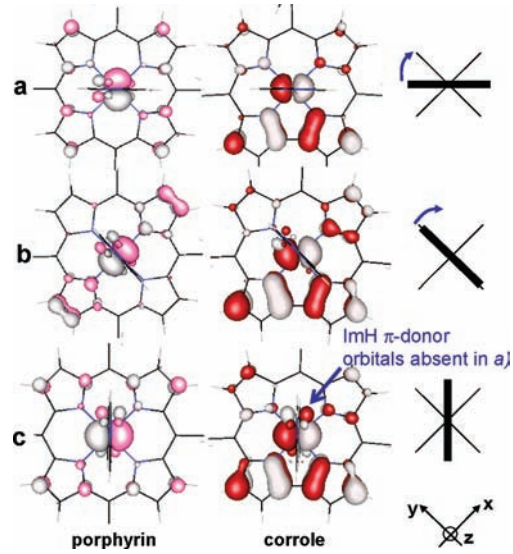

Figure 8. Fe(III) porphyrin and corrole d_π LUMO delocalization as a function of axial ligand orientation. a) ImH ligands eclipsed and oriented to bisect the x,y axis, b) ImH ligands eclipsed and along the y axis, and c) ImH rotated 90° to orientation in a) and bisecting the ring contracted direction. To the right, the black rectangles intersecting the black cross indicate the orientation of the axial ImH relative to the porphyrin ring.

The fixed orientation of the Fe d_π β LUMO in Fe(III) corrole has a significant effect on the π-donor interaction of the axial ligand. In Figure 8, right, the ImH π-donor orbitals do not contribute to the LUMO in a) (ImH π coplanar with $d_{xz} + d_{yz}$) but start to contribute in b) and strongly contribute in c) (ImH π coplanar with $d_{yz} - d_{xz}$), as indicated by the blue arrow. However, in c) the ImH is not in the orientation that is observed experimentally. This is because there is a steric preference for the plane of the ring to orient such that it does not intersect the contracted side of the corrole ring (molecular mechanics calculations in Figure S12 in the Supporting Information).

One of the significant differences between Fe(III) porphyrin and corrole complexes is the marked axial lability observed in the iron corroles relative to the iron porphyrinates.[77] To explore the origin of this difference, a set of calculations was done to examine the energy differences between 5- and 6-coordinate ferric corrole and porphyrin with axial pyridines. We find that the axial ligand bond dissociation energy for Fe(III) corrole is 8 kcal/mol (33.4 kJ/mol)

(77) Joseph, C. A.; Ford, P. C. *J. Am. Chem. Soc.* **2005**, *127*, 6737–6743.

(78) Note that there is not a significant difference in the energies calculated between a high-spin and low-spin $[Fe^{III}(porphyrin)py]^+$ product.

(79) Note that ImH is used here for direct comparison; however, Figure S11 in the Supporting Information shows that axial py has the same effect.

significantly smaller than the 15 kcal/mol (62.7 kJ/mol) calculated for the Fe(III) porphyrin.[80] Consistent with these calculations, it is often found experimentally that the axial Fe^{III}−corrole distances are longer than in the analogous Fe(III) porphyrin complexes. For py, the calculated bond distances are: 2.072 Å (corrole) and 2.038 Å (porphyrin). From crystallography the Fe^{III}−py distances are 2.03 Å[81,82] in[Fe(tpfc)py_2] and 2.00 Å[29] in an analogous porphyrin compound [Fe(tpp)py_2]Cl. There is no experimental comparison for ImH. In addition, there have been numerous reports of axial lability in Fe(III) corrole complexes.[77,83,84] This study defines two contributions to the axial ligand lability in metallocorroles: 1) the ring contraction of the corrole increases the σ and π equatorial donor strength, and 2) the contracted corrole sterically orients the planar axial ligands such that they cannot π donate into the d_π β LUMO. These effects result in both reduced σ- and π-donation of the axial ligand in corrole relative to porphyrin complexes.

In summary, we have quantified the covalency and the ligand field splitting of Fe(III) d-orbitals by the corrole macrocycle. This has allowed the identification of contributions to the axial lability observed in ferric corrole complexes. These are a decrease in σ-donation into d_{z^2} by the axial ligand due to the competition with σ donation by the corrole and a loss of π-donor strength due to the locked-in orientation of the d_π hole by the contracted corrole (Figure 8, right) such that it cannot interact with the planar axial ligand when oriented to avoid the ring contracted direction.

Acknowledgment. This work was supported by grants from the NIH GM-40392 and NSF CHE-0446304 to E.I.S., NIH RR-01209 to K.O.H., NIH DK-31038 to F.A.W, and the ISF to Z.G. This work was performed at SSRL, which is funded by the DOE Office of Basic Energy Sciences. The SSRL Structural Molecular Biology Program is supported by the NIH National Center for Research Resources, Biomedical Technology Program and by the DOE Office of Biological and Environmental Research.

Supporting Information Available: Complete versions of refs 33 and 35; complete version of the data collected for [Fe(tdcc)py_2[and [Fe(tpfcc)py_2] at both the Fe K and L edge; examination of the implications of D_{4h} versus C_{2v} for VBCI modeling; examination of the effects of initial state versus final state parameters on spectral shape; complete version of Figure 3 including isodensities for the orbitals that do not interact with the metal; orbital energies and isodensities for the pair of ImH and Py orbitals; Figure 4 repeated showing the σ bonding orbitals of heme and corrole; plot that shows the spectral effects of differential orbital covalency; superposition of experimental and simulated data for the Fe K pre-edges of ferric porphyrin and corrole; isodensities that show the effect on the LUMO for different orientations of both py and ImH; outputs from an NPA population analysis on each [Fe(tpp)$(ImH)_2$]$^+$ and [Fe-(tdcc)py_2]; finally, a molecular mechanics analysis of the steric effects of different ring orientations. This material is available free of charge via the Internet at http://pubs.acs.org.

IC802248T

(80) Note that there is not a significant difference in the energies calculated between high-spin and low-spin [Fe^{III}(porphyrin)py]$^+$ product.

(81) Naiyin Li.; Petricek, V.; Coppens, P.; Landrum, J. *Acta Crystallogr.* **1985**, *C41*, 902–04.
(82) Inniss, D.; Solts, S. M.; Strouse, C. E. *J. Am. Chem. Soc.* **1988**, *110*, 5644–5654.
(83) Mahammed, A.; Giladi, I.; Goldberg, I.; Gross, Z. *Chem.—Eur. J.* **2001**, 4259–4265.
(84) Aviv, I.; Gross, Z. *Chem.—Eur. J.* **2008**, *14*, 3995–4005.